Dalton Transactions

Cite this: *Dalton Trans.*, 2012, **41**, 9532

www.rsc.org/dalton

PAPER

Syntheses, crystal structures and properties of new lead(II) or bismuth(III) selenites and tellurite†

Su-Yun Zhang,[a,b] Chun-Li Hu,[a] Pei-Xin Li,[a] Hai-Long Jiang[a] and Jiang-Gao Mao*[a]

Received 9th March 2012, Accepted 6th June 2012
DOI: 10.1039/c2dt30560g

Four new lead(II) or bismuth(III) selenites and a tellurite, namely, $Pb_3(TeO_3)Cl_4$, $Pb_3(SeO_3)_2Br_2$, $Pb_2Cd_3(SeO_3)_4I_2(H_2O)$, $Pb_2Ge(SeO_3)_4$ and $BiFe(SeO_3)_3$, have been prepared and structurally characterized by single crystal X-ray diffraction (XRD) analyses. These compounds exhibit five different types of structures. The structure of $Pb_3(TeO_3)Cl_4$ features a three-dimensional (3D) lead(II) chloride network with tellurite anions filling in the 1D tunnels of Pb_4 4-member rings (MRs) along the *c*-axis. $Pb_3(SeO_3)_2Br_2$ contains a 3D network composed of lead(II) selenite layers interconnected by bromide anions. $Pb_2Cd_3(SeO_3)_4I_2(H_2O)$ is a 3D structure based on 2D cadmium(II) selenite layers which are further connected by 1D lead(II) iodide ladder chains with lattice water molecules located at the 1D tunnels of the structure. $Pb_2Ge(SeO_3)_4$ features a 3D framework constructed by the alternate arrangement of lead(II) selenite layers and germanium(IV) selenite layers in the [100] direction. The structure of $BiFe(SeO_3)_3$ is built on the 3D anionic framework of ion(III) selenite with the bismuth(III) ions located at its Fe_6Se_6 12-MR tunnels. $Pb_3(TeO_3)Cl_4$ ($Pna2_1$) is polar and $BiFe(SeO_3)_3$ ($P2_12_12_1$) is noncentrosymmetric. Powder second-harmonic generation (SHG) measurements using 1064 nm radiation indicate that $BiFe(SeO_3)_3$ exhibits a weak SHG efficiency of about 0.2 × KH_2PO_4 (KDP). Magnetic property measurements for $BiFe(SeO_3)_3$ show a dominant antiferromagnetic interaction with weak spin-canting at low temperatures. IR, UV-vis and thermogravimetric, as well as electronic structure calculations were also performed.

Introduction

Metal selenites and tellurites can form a diversity of unusual structures due to the presence of the stereochemically active lone-pair electrons in Se^{4+} and Te^{4+} cations, which can serve as structure-directing agents.[1] The asymmetric coordination polyhedron of the Se^{4+} or Te^{4+} atom caused by the so-called second-order Jahn–Teller (SOJT) distortion may also result in noncentrosymmetric (NCS) structures with consequent interesting physical properties, such as non-linear optical SHG, piezoelectric, ferroelectric and pyroelectric properties.[2] Transition metal ions with d^0 electronic configurations, such as V^{5+}, $Mo^{6+}$and Ti^{4+}, which are also susceptible to SOJT distortion, have been introduced to metal selenites and tellurites to reinforce the polarization of these structures by additive polarization from both types of asymmetric polyhedra.[3] So far, a large number of compounds combining the above two types of cations have been synthesized and the counter-cations used to balance the excess negative charges of the anionic architectures include alkaline or NH_4^+ ions,[4] alkaline-earth ions,[5] transition-metal ions,[6,7] post-transition metal main-group IIIA cations (such as Ga^{3+}/In^{3+})[8] and lanthanide(III) ions.[9] Borate anions have also been introduced into selenites by our group, which led to the discovery of a new type of second-order NLO compound, $Se_2B_2O_7$.[2c]

It is reported that the combination of two types of lone-pair containing cations can also afford new phases with novel structures and interesting properties, for example, Bi_2TeO_5, Pb_3SeO_5 and $TeSeO_4$ display large SHG responses of 300 × α-SiO_2, 300 × α-SiO_2 and 400 × α-SiO_2, respectively.[10] Lead(II) and bismuth(III) selenites or tellurites with a transition metal ion or a group IV cation are expected to display novel inorganic structures due to the presence of three types of structural building units. To the best of our knowledge, no Pb(II)/Bi(III)–Ge(IV)–Se(IV)/Te(IV)–O phase has been found and only a few quaternary or pentanary Pb(II)/Bi(III)–Cu(II)/Fe(III)–Se(IV)/Te(IV)–O phases have been isolated:[11,12] $PbCuTe_2O_7$, $PbCu_2(SeO_3)_3$, $PbFe_2(SeO_3)_4$, $Bi_2Cu(SeO_3)_4$, $Bi_2OCu(SeO_3)_3(H_2O)$, $Cu_6PbO_2(SeO_3)_2Cl_5$, $BiCu_3$-

[a]*State Key Laboratory of Structural Chemistry, Fujian Institute of Research on the Structure of Matter, Chinese Academy of Sciences, Fuzhou 350002, P. R. China. E-mail: mjg@fjirsm.ac.cn*
[b]*Graduate School of the Chinese Academy of Sciences, Beijing 100039, P. R. China*

†Electronic supplementary information (ESI) available: X-ray crystallographic files in CIF format, energy-dispersive X-ray spectroscopy, simulated and experimental XRD patterns, IR, UV absorption, optical diffuse reflectance spectra, orientations of TeO_3 in $Pb_3(TeO_3)Cl_4$ and SeO_3 in $BiFe(SeO_3)_3$, magnetic susceptibility at different fields, band structures and total and partial densities of states (TDOS and PDOS), the TGA diagram of $Pb_2Cd_3(SeO_3)_4I_2(H_2O)$ and the enlarged TGA diagram between 30–120 °C. CSD 424284–424288. For ESI and crystallographic data in CIF or other electronic format see DOI: 10.1039/c2dt30560g

$(SeO_3)_2O_2X$ (X = Cl, Br, I) and $BiCu_3(TeO_3)_2O_2Cl$. The incorporation of Cu^{2+} or Fe^{3+} ions has greatly enriched the diversity of their structures.

It is reported that the combination of Se^{4+} (or Te^{4+}) and a halide anion may form low dimensional structures because both of them can act as "chemical scissors".[13] Such a synthetic concept has resulted in the isolation of many low-dimensional transition metal compounds with interesting magnetic properties.[14] As for the halides of lead(II) (or bismuth(III)) selenites (or tellurites), the structurally characterized phases include $Pb_3TeO_4X_2$ (X = Cl, Br, I), $Pb_3(SeO_3)Cl_4(H_2O)$, $Pb_3(SeO_3)_2Cl_2$, $Pb_3Te_2O_6X_2$ (X = Cl, Br), $Bi(SeO_3)Cl$, $Bi(TeO_3)I$, $Bi_4Te_2O_9Br_2$, $Bi_5TeO_{8.5}Br_2$, $Bi_5TeO_{8.5}I_2$, $Bi_3Te_4O_{10}Cl_5$ and $Bi_8(SeO_3)_9Br_6$.[15,16] In all these compounds, the Se(IV) and Te(IV) cations form bonds with only oxygen, whereas lead(II) and bismuth(III) can form bonds with both halogen and oxygen atoms. Most of these studies focused on the tellurite system whereas the corresponding selenite system has been hardly explored. Based on the above ideas, we started a research program to systematically explore lead(II)/bismuth(III) selenites/tellurites mixed with additional metal ions or halide anions. Such efforts led to the isolation of five new compounds, namely, $Pb_3(TeO_3)Cl_4$, $Pb_3(SeO_3)_2Br_2$, $Pb_2Cd_3(SeO_3)_4I_2(H_2O)$, $Pb_2Ge(SeO_3)_4$ and $BiFe(SeO_3)_3$. Herein we report their syntheses, crystal structures and physical properties.

Experimental

Materials and instrumentation

All of the chemicals were analytically pure from commercial sources and were used without further purification. $PbCl_2$, PbO, Ga_2O_3, $Pb(NO_3)_2$, KBr, GeO_2, CdI_2, Bi_2O_3 and $FeCl_3{\cdot}6H_2O$ were purchased from the Shanghai Reagent Factory (AR, 90.0+%); SeO_2 (99+%) and TeO_2 (99+%) were purchased from ACROS ORGANICS. Fourier transform infrared (FT-IR) spectra (KBr pellets) were recorded on a Bomen MB-102 FT-IR spectrometer. Microprobe elemental analyses were performed on a field emission scanning electron microscope (FESEM, JSM6700F) equipped with an energy dispersive X-ray spectroscope (EDS, Oxford INCA). The X-ray powder diffraction data were collected on a MiniFlex diffractometer using graphite-monochromated CuKa radiation in the 2θ range of 5–65°. Optical diffuse reflectance spectra were measured at room temperature with a PE Lambda 900 UV-Visible spectrophotometer. $BaSO_4$ plate was used as a standard (100% reflectance). The absorption spectrum was calculated from reflectance spectra using the Kubelka–Munk function: $\alpha/S = (1 - R)^2/2R$,[17] where α is the absorption coefficient, S is the scattering coefficient, which is practically wavelength independent when the particle size is larger than 5 μm, and R is the reflectance. Thermogravimetric analyses were carried out with a NETZSCH STA 449C unit at a heating rate of 10 °C min^{-1} from room temperature to 1000 °C under a N_2 atmosphere. The measurements of the powder frequency-doubling effects were carried out by means of the method of Kutz and Perry.[18] The fundamental wavelength, generated by a Q-switched Nd:YAG laser, is 1064 nm. The SHG wavelength is 532 nm and KDP was used as the reference to assume the effect. Magnetic susceptibility measurements on polycrystalline samples were performed with a PPMS-9T magnetometer at a field of 1000 Oe in the temperature range of 2–300 K. The raw data were corrected for the susceptibility of the container and the diamagnetic contributions of the samples using Pascal's constants.[19]

Syntheses of the title compounds

Preparation of $Pb_3(TeO_3)Cl_4$. Single crystals of $Pb_3(TeO_3)Cl_4$ were initially obtained along with some unidentified powders, by hydrothermal reactions of a mixture of Ga_2O_3, $PbCl_2$ and TeO_2 in a molar ratio of 1 : 1 : 10 in H_2O (4 mL), which was sealed in an autoclave equipped with a Teflon liner (23 mL) at 230 °C for 4 days, followed by slow cooling to room temperature at a rate of 6 °C h^{-1}. The final pH value of the reaction media was close to 2.0. The EDS elemental analyses on several single crystals gave an average molar ratio for Pb–Te–Cl of 2.8 : 1.0 : 4.1, which is in good agreement with the one determined from single-crystal X-ray structural studies (Fig. S1†). The single phase of $Pb_3(TeO_3)Cl_4$ was obtained in a yield of *ca.* 75% (based on Pb) after washing away the above powders in water by ultrasonic cleaning. Its purity was confirmed by XRD studies (Fig. S2†). IR data (KBr, cm^{-1}): 728 (m), 657 (s), 771 (w), 422(m) (Fig. S3†).

Preparation of $Pb_3(SeO_3)_2Br_2$. A mixture of $Pb(NO_3)_2$ (99.4 mg, 0.3 mmol), KBr (47.6 mg, 0.4 mmol), SeO_2 (66.6 mg, 0.6 mmol) and H_2O (5 mL) was sealed in an autoclave equipped with a Teflon liner (23 mL) and heated at 200 °C for 4 days, followed by slow cooling to room temperature at a rate of 6 °C h^{-1}. Colorless block-shaped crystals of $Pb_3(SeO_3)_2Br_2$ were recovered along with tiny $PbSeO_3$ crystals as an impurity. EDS elemental analyses gave the molar ratio for Pb–Se–Br of 1.6 : 1.0 : 1.2, which is in good agreement with the one determined from single crystal X-ray structural analysis (Fig. S1†). After proper structural analysis, $Pb_3(SeO_3)_2Br_2$ was obtained as a single phase by the hydrothermal reaction of a mixture of $Pb(NO_3)_2$ (99.4 mg, 0.3 mmol), KBr (238.0 mg, 2.0 mmol) and SeO_2 (44.4 mg, 0.4 mmol) in 5 mL H_2O at 200 °C for 4 days. The large excess amount of KBr is needed to prevent the formation of $PbSeO_3$. The yield was *ca.* 39% (based on Pb) and its purity was confirmed by X-ray powder diffraction studies (Fig. S2†). IR data (KBr, cm^{-1}): 823 (s), 699 (s), 621 (s), 458(s) (Fig. S3†).

Preparation of $Pb_2Cd_3(SeO_3)_4I_2(H_2O)$. Brown rod-shaped crystals of $Pb_2Cd_3(SeO_3)_4I_2(H_2O)$ were initially obtained along with crystals of $PbSeO_3$ and $CdSeO_3$ as impurities, by hydrothermal reaction of a mixture containing PbO (22.3 mg, 0.1 mmol), CdI_2 (36.6 mg, 0.1 mmol) and SeO_2 (111.0 mg, 1.0 mmol) in H_2O (4 mL), which was sealed in an autoclave equipped with a Teflon liner (23 mL) and heated at 230 °C for 4 days, followed by slow cooling to room temperature at a rate of 6 °C h^{-1}. The final pH value of the reaction media was close to 1.0. EDS elemental analyses on several single crystals gave an average molar ratio for Pb–Cd–Se–I of 1.0 : 1.6 : 2.3 : 1.1, which is in good agreement with the one determined from single-crystal X-ray structural studies (Fig. S1†). After proper structural analysis, a single phase of $Pb_2Cd_3(SeO_3)_4I_2(H_2O)$ was obtained

in a molar ratio of PbO, CdI_2 and SeO_2 of 1 : 2 : 12 under the same reaction conditions in a yield of *ca.* 78% (based on Pb). Its purity was confirmed by XRD studies (Fig. S2†). IR data (KBr, cm^{-1}): 840 (m), 816 (w), 733 (s), 664 (s), 477 (s) (Fig. S3†).

Preparation of $Pb_2Ge(SeO_3)_4$. A mixture of PbO (44.6 mg, 0.2 mmol), GeO_2 (10.5 mg, 0.1 mmol), SeO_2 (222.0 mg, 2.0 mmol) and H_2O (4 mL) was sealed in an autoclave equipped with a Teflon liner (23 mL) and heated at 200 °C for 4 days, and then cooled to room temperature at a rate of 6 °C h^{-1}. The final pH value of the reaction media is close to 0.5. The product was washed with water, and then dried in air. Colorless prism-shaped crystals of $Pb_2Ge(SeO_3)_4$ were obtained as a single phase in a yield of *ca.* 51% based on Pb. Its purity was confirmed by XRD studies (Fig. S2†). EDS elemental analyses on several single crystals of $Pb_2Ge(SeO_3)_4$ gave an average molar ratio for Pb–Ge–Se of 2.1 : 1.0 : 3.9, which is in good agreement with the one determined from single-crystal X-ray structural studies (Fig. S1†). IR data (KBr cm^{-1}): 827 (w), 727 (m), 687 (s), 543 (s), 503 (m), 420 (s) (Fig. S3†).

Preparation of $BiFe(SeO_3)_3$. Green rod-shaped crystals of $BiFe(SeO_3)_3$ were initially prepared by the high temperature solid-state reaction of a mixture containing BiOCl, Bi_2O_3 and SeO_2 in a molar ratio of 3 : 2 : 2. The reaction mixture was thoroughly ground and pressed into a pellet, which was then sealed into an evacuated quartz tube. The sample was allowed to heat at 300 °C for 1 day, then at 700 °C for 6 days, followed by cooling to 350 °C at 3.5 °C h^{-1} before switching off the furnace. EDS elemental analysis gave the molar ratio for Bi–Fe–Se of 1.0 : 1.1 : 3.1, which matches well with the one from single crystal X-ray structural analysis (Fig. S1†). The Fe^{3+} in the compound maybe come from iron rust on the mold in the process of pressing the reaction mixture into a pellet. A pure sample of $BiFe(SeO_3)_3$ was obtained by hydrothermal reaction of a mixture of Bi_2O_3 (23.3 mg, 0.05 mmol), $FeCl_3{\cdot}6H_2O$ (27.0 mg, 0.1 mmol) and SeO_2 (177.6 mg, 1.6 mmol), which was sealed in an autoclave equipped with a Teflon liner (23 mL) and heated at 230 °C for 4 days, and then cooled to room temperature at a rate of 6 °C h^{-1}. The yield is about 77% based on Bi. Its purity was confirmed by X-ray powder diffraction studies (Fig. S2†). IR data (KBr, cm^{-1}): 871 (s), 836 (m), 752 (s), 705 (w), 663(m), 502(s) (Fig. S3†).

Single-crystal structure determination

Data collections for the above five compounds were performed on either a Rigaku SCXMini CCD (for $Pb_3(TeO_3)Cl_4$, $Pb_2Cd_3(SeO_3)_4I_2(H_2O)$ and $BiFe(SeO_3)_3$), a Rigaku Mercury CCD (for $Pb_3(SeO_3)_2Br_2$) or a Saturn 70 (for $Pb_2Ge(SeO_3)_4$) equipped with a graphite-monochromated Mo-Ka radiation (λ = 0.71073 Å) at 293 K. The data sets were corrected for Lorentz and polarization factors as well as for absorption by the multi-scan method.[20a] All five structures were solved by direct methods and refined by full-matrix least-squares fitting on F^2 by SHELX-97.[20b] All non-hydrogen atoms were refined with anisotropic thermal parameters. All oxygen atoms in $Pb_3(TeO_3)Cl_4$ and $Pb_3(SeO_3)_2Br_2$, O1, O2 and O5 in $Pb_2Ge(SeO_3)_4$ and O2, O7 and O8 in $BiFe(SeO_3)_3$ were refined with restraints of SIMU and ISOR because of their very small ADP volumes. O1W in $Pb_2Cd_3(SeO_3)_4I_2(H_2O)$ was refined with ISOR 0.001 O1W because of its large thermal parameter. In $Pb_3(TeO_3)Cl_4$, the highest peak of 3.65 $Å^{-3}$ is 1.20 Å from Te(1) and the deepest hole of −3.66 $Å^{-3}$ is 0.86 Å from Pb(3). In $Pb_3(SeO_3)_2Br_2$, the highest peak of 3.77 $Å^{-3}$ is 0.88 Å from Pb(1) and the deepest hole of −3.64 $Å^{-3}$ is 0.84 Å from Pb(2). In $Pb_2Cd_3(SeO_3)_4I_2(H_2O)$, the highest peak of 1.43 $Å^{-3}$ is 0.61 Å from Cd(1) and the deepest hole of −3.42 $Å^{-3}$ is 0.74 Å from Pb(1). In $BiFe(SeO_3)_3$, the highest peak of 1.98 $Å^{-3}$ is 1.35 Å from Bi(1) and the deepest hole of − 1.99 $Å^{-3}$ is 0.98 Å from Bi(1). All these residuals can be regarded as ghost peaks. The information of the restraints and the positions of these peaks has been given in the CIF files. The refined Flack factors of 0.011(11) and −0.031(10) respectively for $Pb_3(TeO_3)Cl_4$ and $BiFe(SeO_3)_3$ confirmed the correctness of their absolute structures. The structures were also checked for possible missing symmetry with PLATON.[20c] Crystallographic data and structural refinements for the five compounds are summarized in Table 1. Important bond distances are listed in Table 2. Further details of the crystal structure studies can be obtained from the Fachinformationszentrum Karlsruhe, 76344 Eggenstein-Leopoldshafen, Germany (Fax: (49) 7247808666; crysdata@fiz-karlsruhe.de), on quoting the depository numbers CSD 424284–424288.

Computational descriptions

Single-crystal structural data of the five compounds were used for the theoretical calculations. The *ab initio* band structure calculations and density of states (DOS) were performed by using the computer code CASTEP.[21] The code employs density functional theory (DFT) using a plane wave basis set with Vanderbilt norm-conserving pseudopotentials to approximate the interactions between the core and valence electrons.[22] The exchange-correlation energy was calculated using the Perdew–Burke–Ernzerh modification to the generalized gradient approximation (GGA).[23] The number of plane waves included in the basis set is determined by a kinetic-energy cutoff of 700 eV for $Pb_3(TeO_3)Cl_4$ and $Pb_2Ge(SeO_3)_4$, 820 eV for $Pb_3(SeO_3)_2Br_2$ and $Pb_2Cd_3(SeO_3)_4I_2(H_2O)$ and 500 eV for $BiFe(SeO_3)_3$. The numerical integration of the Brillouin zone is performed by using 3 × 2 × 3, 3 × 3 × 1, 3 × 1 × 1, 3 × 4 × 3, and 3 × 3 × 2 Monkhorst-Pack k-point sampling for the five compounds, respectively. Pseudoatomic calculations were performed for O $2s^22p^4$, Se $4s^24p^4$, Te $5s^25p^4$, Pb $5d^{10}6s^26p^2$, Bi $5d^{10}6s^26p^3$, Ge $4s^24p^2$, Fe $3d^64s^2$, Cl $3s^23p^5$, Br $4s^24p^5$ and I $5s^25p^5$. Spin polarization was included for the electronic structure calculations of $BiFe(SeO_3)_3$. The other calculating parameters used in the calculations and convergent criteria were set by the default values of the CASTEP code.

Results and discussion

Four new lead(II) and bismuth(III) selenites and a tellurite with additional halide anions or metal ions, namely, $Pb_3(TeO_3)Cl_4$, $Pb_3(SeO_3)_2Br_2$, $Pb_2Cd_3(SeO_3)_4I_2(H_2O)$, $Pb_2Ge(SeO_3)_4$ and $BiFe(SeO_3)_3$, have been successfully synthesized through

Table 1 Crystal data and structure refinements for the five compounds

Formula	$Pb_3(TeO_3)Cl_4$	$Pb_3(SeO_3)_2Br_2$	$Pb_2Cd_3(SeO_3)_4I_2(H_2O)$	$Pb_2Ge(SeO_3)_4$	$BiFe(SeO_3)_3$
F_w	938.97	1035.31	1531.24	994.81	645.71
Space group	$Pna2_1$	$C2/c$	$P2/c$	$P2(1)/c$	$P2_12_12_1$
a/Å	7.427(4)	13.4369(17)	11.200(9)	8.971(5)	7.615(3)
b/Å	15.993(8)	5.6626(8)	5.439(4)	6.633(3)	8.702(3)
c/Å	8.483(4)	13.321(2)	16.649(10)	9.256(5)	12.668(5)
α/°	90	90	90	90	90
β/°	90	92.995(9)	119.24(4)	96.376(9)	90
γ/°	90	90	90	90	90
V/Å^3	1007.5(9)	1012.2(2)	885.0(11)	547.4(5)	839.4(5)
Z	4	4	2	2	4
D_{calcd}/g cm^{-3}	6.190	6.794	5.746	6.036	5.110
M(Mo-Ka)/mm^{-1}	53.861	64.857	34.275	46.774	35.699
R_{int}	0.0672	0.0463	0.0476	0.0231	0.0714
GOF on F^2	0.994	1.111	1.035	1.021	0.894
Flack factor	0.010(10)	N/A	N/A	N/A	−0.031(10)
R_1, wR_2 $[I > 2\sigma(I)]^a$	0.0375, 0.0770	0.0350, 0.0810	0.0380, 0.0853	0.0157, 0.0366	0.0343, 0.0606
R_1, wR_2 (all data)	0.0420, 0.0783	0.0377, 0.0818	0.0502, 0.0910	0.0179, 0.0372	0.0358, 0.0613

$R_1 = \sum||F_o| - |F_c||/\sum|F_o|$, $wR_2 = \{\sum w[(F_o)^2 - (F_c)^2]^2/\sum w[(F_o)^2]^2\}^{1/2}$.

hydrothermal reactions. They belong to five different types of structures. In $Pb_3(TeO_3)Cl_4$, $Pb_3(SeO_3)_2Br_2$ and $Pb_2Cd_3(SeO_3)_4I_2(H_2O)$, the halide anions are coordinated to Pb^{2+} forming oxyhalide polyhedra, the latter of which are further connected into 3D networks or 1D chains, whereas the metal ions in $Pb_2Cd_3(SeO_3)_4I_2(H_2O)$, $Pb_2Ge(SeO_3)_4$and $BiFe(SeO_3)_3$ are bridged by SeO_3^{2-} anions into 2D layers or 3D frameworks.

Structural descriptions

Structure of $Pb_3(TeO_3)Cl_4$. The structure of $Pb_3(TeO_3)Cl_4$ features a 3D lead(II) chloride network with tellurite anions filling in the 1D tunnels of Pb_4-MRs along the c-axis (Fig. 1a). The asymmetric unit of $Pb_3(TeO_3)Cl_4$ contains three Pb^{2+} cations, one TeO_3^{2-} anion and four chloride anions. All three Pb^{2+} cations are surrounded by oxo and halide anions. Pb(1) is seven-coordinated by three oxygen atoms from two tellurite groups and four chloride anions. The Pb(2) atom is seven-coordinated by one TeO_3^{2-} in a bidentate chelating fashion and five chloride anions, whereas Pb(3) is seven-coordinated by two oxygen atoms from two TeO_3^{2-} anions in a unidentate fashion and five chloride anions. The coordination environments around Pb atoms demonstrate that the lone pairs of the Pb atoms are not optically active. The Pb–O distances are in the range of 2.322(13)–2.575(15) Å and those of Pb–Cl bonds fall in the range of 2.804(5)–3.309(5) Å (Table 2), which are close to those reported in the other lead(II) tellurite oxychlorides.[15a,b] The Te(IV) atom is three-coordinated by three oxygen atoms in a distorted ψ-TeO_3 tetrahedral geometry, with the fourth site occupied by the lone-pair electrons as in other metal tellurites reported previously. The Te–O distances fall in the range of 1.851(12) and 1.890(10) Å (Table 2). Bond valences sum (BVS) calculations gave total bond valences of 3.98, 2.08, 2.37 and 2.18, respectively for Te(1), Pb(1), Pb(2) and Pb(3), indicating an oxidation state of +4 and +2 for Te and Pb atoms, respectively.[24]

The interconnection of lead(II) ions by bridging chloride ions led to the formation of a lead(II) chloride 3D network with 4- and 6-MR tunnels along the c-axis (Fig. 1b). Cl(1) and Cl(2) each bond with two lead(II) ions whereas Cl(3) and Cl(4) link with four lead(II) ions. The tellurite anions are grafted into the 4-MR tunnels. Each tellurite anion forms a bidentate chelation with Pb(1) and Pb(2) and, in addition, they are also bonded to one Pb(1) and two Pb(3) atoms. Hence, the lead(II) ions are bridged by tellurite anions into a 1D chain along the c-axis (Fig. 1c).

Structure of $Pb_3(SeO_3)_2Br_2$. $Pb_3(SeO_3)_2Br_2$ is isostructural with the previously reported $Pb_3(SeO_3)_2Cl_2$.[15c] It contains a 3D network composed of lead(II) selenite layers interconnected by bromide anions (Fig. 2a). There are two Pb^{2+} ions (one on a mirror plane and one at a general site), one SeO_3^{2-} anion and one bromide anion in the asymmetric unit. Both Pb(1) and Pb(2) atoms are eight-coordinated. Pb(1) is surrounded by two bromide anions and six oxygen atoms from two unidentate and two bidentate SeO_3^{2-} anions, whereas Pb(2) is bonded to three bromide and five O^{2-} anions from three unidentate and one bidentate SeO_3^{2-} anions. The oxygen atoms and bromide anions distribute around the Pb atoms, suggesting that the lone pairs of Pb^{2+} ions are inert. The Pb–O distances range from 2.519(7) to 2.786(8) Å and the Pb–Br distances fall in the range of 3.1025(12) to 3.3057(12) Å (Table 2). The Se(IV) cation is in a distorted ψ-SeO_3 tetrahedral geometry, with the fourth site occupied by the lone-pair electrons. The Se–O distances fall in the range of 1.654(9) to 1.737(8) Å (Table 2). Results of BVS calculations indicate that the Se and Pb atoms are in oxidation states of +4 and +2, respectively. The calculated total bond valences are 4.22, 1.75 and 2.00, respectively for Se(1), Pb(1) and Pb(2).[24]

The interconnection of lead(II) ions by bridging selenite anions led to the formation of a 2D layer perpendicular to the c-axis (Fig. 2b). Each selenite anion forms two Pb–O–Se–O chelation rings with two lead(II) ions and is also bridged to four other lead(II) ions. Two oxygen atoms are tridentate whereas the third one is bidentate. These lead(II) selenite layers are further interconnected by bromide anions into a 3D network. Each bromide anion is tetradentate and bonds with four lead(II) ions

Table 2 Important bond lengths (Å) for the five compounds

		$Pb_3(TeO_3)Cl_4$[a]	
Pb(1)–O(3)#1	2.322(13)	Pb(1)–O(1)	2.475(10)
Pb(1)–O(2)	2.575(16)	Pb(1)–Cl(1)	2.921(5)
Pb(1)–Cl(3)#2	3.104(4)	Pb(1)–Cl(2)#3	3.173(5)
Pb(1)–Cl(2)#4	3.309(5)	Pb(2)–O(3)	2.436(12)
Pb(2)–Cl(2)	2.804(5)	Pb(2)–Cl(4)#5	2.979(5)
Pb(2)–Cl(3)	3.008(4)	Pb(2)–Cl(3)#6	3.097(5)
Pb(2)–Cl(4)#7	3.097(5)	Pb(3)–O(2)#8	2.393(11)
Pb(3)–O(1)#9	2.476(10)	Pb(3)–Cl(1)#9	2.838(5)
Pb(3)–Cl(4)	2.981(4)	Pb(3)–Cl(3)	3.022(4)
Pb(3)–Cl(4)#6	3.179(5)	Pb(3)–Cl(3)#6	3.190(5)
Te(1)–O(2)	1.851(13)	Te(1)–O(3)	1.879(13)
Te(1)–O(1)	1.890(10)		
		$Pb_3(SeO_3)_2Br_2$[b]	
Pb(1)–O(1)#1	2.603(7)	Pb(1)–O(1)	2.603(7)
Pb(1)–O(2)#2	2.729(8)	Pb(1)–O(2)#3	2.729(8)
Pb(1)–O(3)#4	2.786(8)	Pb(1)–O(3)#1	2.786(8)
Pb(1)–Br(1)#1	3.1425(12)	Pb(1)–Br(1)	3.1425(12)
Pb(2)–O(1)#5	2.519(7)	Pb(2)–O(2)#3	2.563(7)
Pb(2)–O(1)#3	2.573(7)	Pb(2)–O(3)#2	2.603(9)
Pb(2)–O(2)#6	2.715(7)	Pb(2)–Br(1)	3.1025(12)
Pb(2)–Br(1)#7	3.2942(12)	Pb(2)–Br(1)#2	3.3057(12)
Se(1)–O(3)	1.654(9)	Se(1)–O(2)	1.708(8)
Se(1)–O(1)	1.737(8)		
		$Pb_2Cd_3(SeO_3)_4I_2(H_2O)$[c]	
Pb(1)–O(4)	2.460(6)	Pb(1)–O(2)	2.474(6)
Pb(1)–O(3)	2.600(6)	Pb(1)–O(5)	2.613(7)
Pb(1)–I(1)	3.424(2)	Pb(1)–I(1)#1	3.465(2)
Pb(1)–I(1)#2	3.523(2)	Cd(1)–O(1)#3	2.279(6)
Cd(1)–O(1)	2.279(6)	Cd(1)–O(5)#4	2.417(6)
Cd(1)–O(5)#5	2.417(6)	Cd(1)–O(4)#4	2.455(7)
Cd(1)–O(4)#5	2.455(7)	Cd(1)–O(6)#6	2.641(9)
Cd(1)–O(6)#7	2.641(9)	Cd(2)–O(6)#8	2.265(8)
Cd(2)–O(2)	2.298(6)	Cd(2)–O(3)#5	2.339(6)
Cd(2)–O(1)#5	2.370(6)	Cd(2)–O(4)#1	2.400(6)
Cd(2)–O(5)	2.624(7)	Cd(2)–O(2)#5	2.638(6)
Cd(2)–O(3)#1	2.825(7)	Se(1)–O(1)	1.677(6)
Se(1)–O(3)#1	1.694(6)	Se(1)–O(2)	1.729(6)
Se(2)–O(6)	1.667(7)	Se(2)–O(5)	1.712(6)
Se(2)–O(4)#1	1.731(6)		
		$Pb_2Ge(SeO_3)_4$[d]	
Pb(1)–O(5)#1	2.345(3)	Pb(1)–O(4)	2.402(3)
Pb(1)–O(5)#2	2.507(3)	Pb(1)–O(3)	2.543(3)
Pb(1)–O(3)#2	2.780(3)	Ge(1)–O(1)#2	1.870(3)
Ge(1)–O(1)#3	1.870(3)	Ge(1)–O(6)#4	1.892(3)
Ge(1)–O(6)#5	1.892(3)	Ge(1)–O(2)#6	1.920(3)
Ge(1)–O(2)	1.920(3)	Se(1)–O(3)	1.673(3)
Se(1)–O(2)	1.734(3)	Se(1)–O(1)	1.743(3)
Se(2)–O(4)	1.687(3)	Se(2)–O(5)	1.703(3)
Se(2)–O(6)	1.729(3)		
		$BiFe(SeO_3)_3$[e]	
Bi(1)–O(4)	2.196(7)	Bi(1)–O(7)	2.215(7)
Bi(1)–O(3)#1	2.276(7)	Bi(1)–O(5)#1	2.572(7)
Bi(1)–O(7)#1	2.613(7)	Bi(1)–O(3)	2.687(7)
Bi(1)–O(2)	2.720(7)	Fe(1)–O(6)#2	1.986(7)
Fe(1)–O(9)	1.993(7)	Fe(1)–O(8)#3	2.004(7)
Fe(1)–O(1)#1	2.007(7)	Fe(1)–O(2)#4	2.019(7)
Fe(1)–O(5)#5	2.074(7)	Se(1)–O(1)	1.681(7)
Se(1)–O(2)	1.705(7)	Se(1)–O(3)	1.727(7)
Se(2)–O(4)	1.679(7)	Se(2)–O(6)	1.680(7)
Se(2)–O(5)	1.714(6)	Se(3)–O(9)	1.649(7)
Se(3)–O(8)	1.699(6)	Se(3)–O(7)	1.725(7)

[a] Symmetry transformations used to generate equivalent atoms: for $Pb_3(TeO_3)Cl_4$: #1 $-x+1, -y+1, z-1/2$; #2 $-x+3/2, y+1/2, z-1/2$; #3 x, y, z; #4 $-x+2, -y+1, z-1/2$; #5 $x, y, z-1$; #6 $x-1/2, -y+1/2, z$; #7 $x-1/2, -y+1/2, z-1$; #8 $-x+1, -y+1, z+1/2$; #9 $x, y, z+1$. [b] Symmetry transformations used to generate equivalent atoms: for $Pb_3(SeO_3)_2Br_2$: #1 $-x+1, y, -z+1/2$; #2 $x, y-1, z$; #3 $-x+1, y-1, -z+1/2$; #4 x, y, z; #5 $x+1/2, y-1/2, z$; #6 $x+1/2, y-3/2, z$; #7 $-x+3/2, -y-1/2, -z+1$. [c] Symmetry transformations used to generate equivalent atoms: for $Pb_2Cd_3(SeO_3)_4I_2(H_2O)$: #1 $x, y-1, z$; #2 $-x, -y+1, -z-1$; #3 $-x-1, y, -z-1/2$; #4 $x, -y, z+1/2$; #5 $-x-1, -y, -z-1$; #6 $-x-1, -y-1, -z-1$; #7 $x, -y-1, z+1/2$; #8 $-x-1, y, -z-3/2$. [d] Symmetry transformations used to generate equivalent atoms: for $Pb_2Ge(SeO_3)_4$: #1 $-x+1, y+1/2, -z+3/2$; #2 $x, -y+1/2, z-1/2$; #3 $-x, y-1/2, -z+3/2$; #4 $-x+1, y-1/2, -z+3/2$; #5 $x-1, -y+1/2, z-1/2$; #6 $-x, -y, -z+1$. [e] Symmetry transformations used to generate equivalent atoms: for $BiFe(SeO_3)_3$: #1 $x-1/2, -y+1/2, -z+2$; #2 $x, y+1, z$; #3 $x-1/2, -y+3/2, -z+2$; #4 $-x+1/2, -y+1, z+1/2$; #5 $-x+1, y+1/2, -z+5/2$.

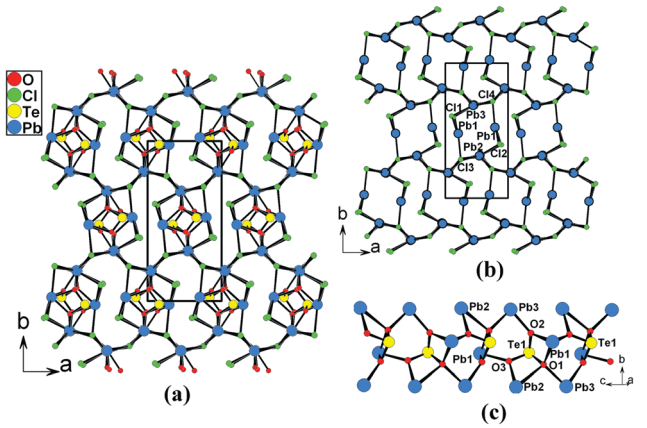

Fig. 1 A view of the structure of $Pb_3(TeO_3)Cl_4$ down the *c*-axis (a), the 3D network of lead(II) chloride (b) and a lead(II) tellurite chain along the *c*-axis (c).

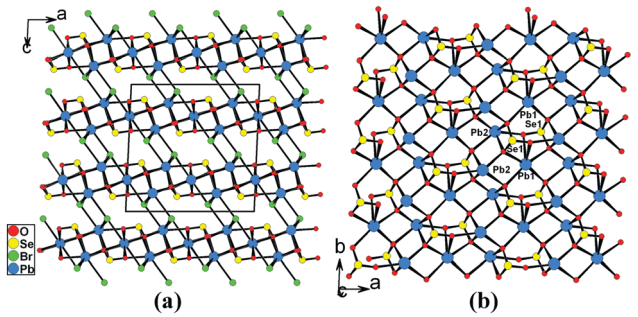

Fig. 2 A view of the structure of $Pb_3(SeO_3)_2Br_2$ down the *b*-axis (a) and a lead(II) selenite layer in the *ab*-plane (b).

from two neighboring layers. The lone pairs of the selenite anions are orientated toward in the interlayer space (Fig. 2a).

It is interesting to compare the structures of $Pb_3(TeO_3)Cl_4$ and $Pb_3(SeO_3)_2Br_2$ with those of $Pb_3(TeO_4)X_2$ (X = Cl, Br, I), $Pb_3(Te_2O_6)X_2$ (X = Cl, Br) and $Pb_3(SeO_3)Cl_4(H_2O)$, which have similar compositions but different structures.[15] Firstly, different lead(II) oxyhalide architectures have been observed. A diversity of lead(II) oxyhalide polyhedra are found in these structures, including PbO_4Cl_4 in $Pb_3(TeO_4)X_2$, PbO_5Cl_3 and PbO_8Cl in $Pb_3(Te_2O_6)X_2$, PbO_5Cl_3 and PbO_4Cl_3 in $Pb_3(SeO_3)Cl_4(H_2O)$, PbO_3Cl_4, $PbOCl_5$ and PbO_2Cl_5 in $Pb_3(SeO_3)Cl_4$ and PbO_6Br_2 and PbO_5Br_3 in $Pb_3(SeO_3)_2Br_2$. These polyhedra are interconnected in different fashions, leading to various lead(II) oxyhalide architectures. Furthermore, tellurium atoms adopt three- or four-coordination whereas selenium atoms are three-coordinated. In $Pb_3(TeO_4)X_2$, TeO_4^{4-} anions are connected into a 1D chain *via* edge-sharing whereas TeO_3^{2-} and $Te_2O_6^{4-}$ of two edge-sharing TeO_4 groups are observed in $Pb_3(Te_2O_6)X_2$.

Structure of $Pb_2Cd_3(SeO_3)_4I_2(H_2O)$. The structure of $Pb_2Cd_3(SeO_3)_4I_2(H_2O)$ features a 3D network based on 2D cadmium(II) selenite layers which are further connected by 1D lead(II) iodide ladder chains (Fig. 3a). Its asymmetric unit contains one Pb^{2+} ion, two Cd^{2+} ions (one at a mirror plane and one at a general site), two selenites anions, one iodide anion and half

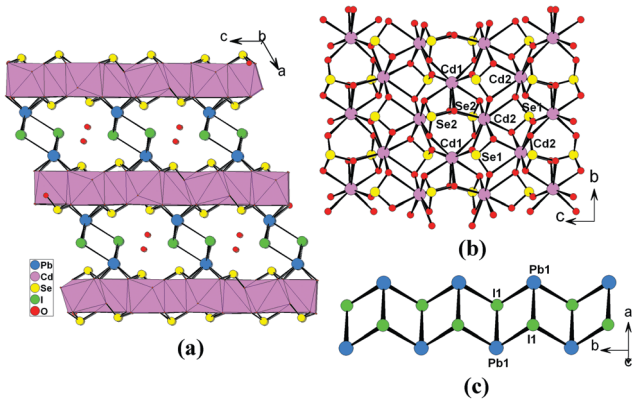

Fig. 3 View of the 3D structure of $Pb_2Cd_3(SeO_3)_4I_2(H_2O)$ down the *b*-axis (a), a cadmium(II) selenite layer parallel to the *bc*-plane (b) and a lead(II) iodide ladder chain along the *b*-axis (c).

a water molecule. The Pb(1) atom is surrounded by four SeO_3^{2-} anions unidentately and three iodide anions. The Pb–O distances range from 2.460(6) to 2.613(7) Å and those of the Pb–I bonds fall in the range of 3.424(2) to 3.523(2) Å (Table 2). Cd(1) is eight-coordinated by two SeO_3^{2-} anions bidentately and four SeO_3^{2-} anions unidentately and Cd(2) is eight-coordinated by three bidentate SeO_3^{2-} and two unidentate SeO_3^{2-} anions. The Cd–O distances range from 2.265(8) to 2.825(7) Å (Table 2). The Se(IV) cations are three-coordinated by three oxygen atoms in a distorted ψ-SeO_3 tetrahedral geometry, with the fourth site occupied by the lone-pair electrons. The Se–O distances fall in the range of 1.667(7) to 1.731(6) Å (Table 2). BVS calculations gave total bond valences of 1.76, 1.95, 1.94, 4.06 and 4.03, respectively for Pb(1), Cd(1), Cd(2), Se(1) and Se(2), indicating oxidation states of +2, +2 and +4, respectively for Pb, Cd and Se.[24]

The interconnection of Cd^{2+} ions by bridging selenite anions led to a 2D layer parallel to the *bc*-plane (Fig. 3b). Each selenite is hexadentate, forming two Cd–O–Se–O chelating rings with two Cd^{2+} ions and also bridges to two other Cd^{2+} ions. The lead(II) ions are bridged by the iodide anions into a ladder chain along the *b*-axis (Fig. 3c). The Pb···Pb separations of the Pb_2I_2 rings are 5.453(11) and 5.455(11) Å (Fig. 3c). Neighboring cadmium (II) selenite layers are further bridged by the lead(II) iodide ladder chains through Pb–O–Se bridges, resulting in the formation of a very complicated 3D framework with 8-MR tunnels of $Pb_4Cd_2Se_2$ along the *b*-axis. The amount of void space is 6.6% using the CALC SOLV command in PLATON. The lattice water molecule located in the tunnels and the lone pairs of Se(1) and Se(2) atoms are orientated toward the center of the tunnels.

The structure of $Pb_2Cd_3(SeO_3)_4I_2(H_2O)$ is different from the pentanary lead(II) and bismuth(III) selenites and tellurites with Cu^{2+}/Cu^{+} and halide anions reported, $PbCu_6O_2(SeO_3)_2Cl_5$, $BiCu_3(SeO_3)_2O_2X$ (X = Cl, Br, I) and $BiCu_3(TeO_3)_2O_2Cl$.[12] In $PbCu_6O_2(SeO_3)_2Cl_5$, the interactions of copper oxyhalide polyhedra and selenite anions result in a 2D layer, which is further linked by lead(II) selenite halide chains into 3D networks. The structures of $BiCu_3(SeO_3)_2O_2X$ are constructed by the alternate arrangement of copper selenite layers and bismuth(III) selenite

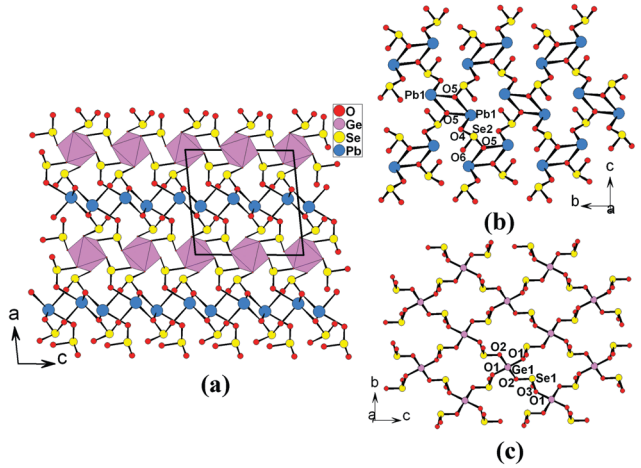

Fig. 4 View of the structure of $Pb_2Ge(SeO_3)_4$ down the *b*-axis (a), a lead(II) selenite layer in the *bc*-plane (b) and a germanium(IV) selenite layer in the *bc*-plane (c).

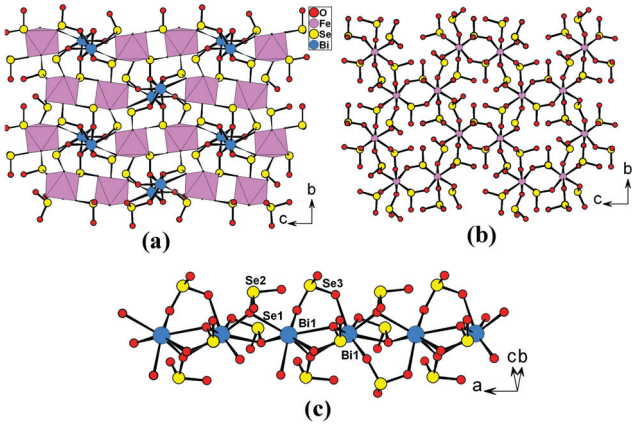

Fig. 5 View of the structure of $BiFe(SeO_3)_3$ down the *a*-axis (a), the 3D iron(III) selenite framework (b) and a 1D bismuth(III) selenite chain along the *a*-axis (c).

layer with the lone-pairs of SeO_3 groups and the dissociative halide anions located in the tunnels of the structure. The structure of $BiCu_3(TeO_3)_2O_2Cl$ is the same as $BiCu_3(SeO_3)_2O_2X$, except that the halide anions coordinate to the Cu^{2+} ions. It can be seen that the main difference is that the Cu^{2+} ions in these compounds are coordinated by oxygen and halide anions, which could be ascribed to the weak Lewis acidity of Cu^{2+} ions.

Structure of $Pb_2Ge(SeO_3)_4$. $Pb_2Ge(SeO_3)_4$ features a 3D framework composed of alternate linkage of lead(II) selenite layers and germanium(IV) selenite layers (Fig. 4a). Its asymmetric unit contains one Pb^{2+} ion, one Ge^{4+} ion (located at a mirror plane) and two selenites anions. Pb(1) atom is five-coordinated by five unidentate SeO_3^{2-} anions with an irregular PbO_5 pyramidal geometry due to the presence of stereoactive lone pairs. The Pb–O distances range from 2.345(3) to 2.780(3) Å (Table 2). The Ge^{4+} ion is octahedrally-coordinated by six oxygen atoms from six unidentate SeO_3^{2-} anions, with the Ge–O distances ranging from 1.870(3) to 1.920(3) Å (Table 2). The Se(IV) cation is asymmetrically coordinated by three oxygen atoms in a distorted ψ-SeO_3 trigonal-pyramidal geometry as a result of its stereoactive lone pairs. The Se–O bond distances fall in the normal range of 1.673(3) to 1.743(3) Å (Table 2). The results of BVS calculations indicate that the Se and Ge atoms are in an oxidation state of +4 with calculated total bond valences of 3.89, 3.99 and 4.05, respectively for Se(1), Se(2) and Ge(1). For Pb(1), the calculated total bond valence is 1.95 with the inclusion of two weak Pb–O interactions (Pb–O(2) 3.026(2) Å and Pb–O(4) 2.986(4) Å).[24]

The lead(II) ions are bridged by tridentate $Se(2)O_3^{2-}$ groups into a 2D lead(II) selenite layer with Pb_2O_2 rings parallel to the *bc*-plane (Fig. 4b). Similarly, the Ge(IV) ions are also bridged by bidentate $Se(1)O_3^{2-}$ anions into a 2D $Ge(SeO_3)_2$ layer, which is also parallel to the *bc*-plane (Fig. 4c). The $Pb(SeO_3)$ and $Ge(SeO_3)_2$ layers are arranged alternately along the *a*-axis and interconnected *via* Se(2)–O(6)–Ge(1) and Se(1)–O(3)–Pb(1) bridges, resulting in a complicated 3D framework (Fig. 4a). The $Se(1)O_3$ group serves as a tetradentate metal linker, connecting with two Ge and two Pb atoms, whereas the $Se(2)O_3$ group is also tetradentate, connecting with one Ge and three Pb atoms.

Structure of $BiFe(SeO_3)_3$. The structure of $BiFe(SeO_3)_3$ is built on the 3D anionic framework of iron(III) selenite with the bismuth(III) ions located at its Fe_6Se_6 12-MR tunnels (Fig. 5a). It contains one Bi^{3+}, one Fe^{3+} and three selenite anions in an asymmetric unit. The Bi(1) atom is seven-coordinated in a distorted pentagonal bipyramidal geometry by five unidentate SeO_3^{2-} and one bidentate SeO_3^{2-} anions. The oxygen atoms distribute around the Bi in a pentagonal bipyramidal geometry, which indicates that lone pairs are inactive. The Bi–O distances range from 2.196(7) to 2.720(7) Å (Table 2), which is similar to those in other bismuth(III) selenites reported previously.[11d,e] Fe(1) is octahedrally-coordinated by six oxygen atoms from six unidentate SeO_3^{2-} anions with the Fe–O distances ranging from 1.986(7) to 2.074(7) Å (Table 2). All three Se(IV) cations are in asymmetric coordination environments due to their stereoactive lone pairs and are bonded by three oxygen atoms. The Se–O bond distances fall in the normal range of 1.649(7) to 1.725(7) Å (Table 2). The results of BVS calculations indicate that the Bi, Fe and Se atoms are in oxidation states of +3, +3 and +4, with calculated total bond valences of 2.97, 2.83, 4.01, 4.15 and 4.17, respectively for Bi(1), Fe(1), Se(1), Se(2) and Se(3) atoms.[24]

The FeO_6 octahedra are connected by bidentate SeO_3^{2-} anions into a 3D network with 1D tunnels of Fe_6Se_6 12-MRs along the *a*-axis (Fig. 5b). Each pair of iron(III) ions are bridged by a pair of selenite anions with Fe···Fe separations in the range of 5.639(2) and 6.191(2) Å. The Bi^{3+} ions are located at the above 12-MR tunnels and are grafted into the above 3D iron(III) selenite network *via* Se–O–Bi bridges. The interconnection of Bi^{3+} ions by bridging selenite anions gave a 1D chain along the *a*-axis (Fig. 5c). $Se(1)O_3$ is pentadentate, forming a bidentate chelation with a Bi atom and also bridges to another Bi and two Fe atoms. $Se(2)O_3$ is tetradentate, bridging with two Bi atoms by using one oxygen atom and two Fe atoms by using two other oxygen atoms. $Se(3)O_3$ is also tetradentate, connecting with one Bi and one Fe atom by using one oxygen atom, and the remaining two oxygen atoms bond to either a Bi or a Fe atom.

The iron(III) selenite anionic framework in $BiFe(SeO_3)_3$ is quite similar to that in the reported $PbFe_2(SeO_3)_4$.[11c] In $PbFe_2(SeO_3)_4$, FeO_6 octahedra are connected by tridentate SeO_3 groups into 3D anionic framework with Pb^{2+} ions in the Fe_4Se_4 8-MR tunnels along the *a*-axis; the SeO_3 groups serve as quadridentate metal linkers, bridging with one Pb and three Fe atoms.

Optical properties

The infrared spectra of $Pb_3(TeO_3)Cl_4$, $Pb_3(SeO_3)_2Br_2$, $Pb_2Cd_3(SeO_3)_4I_2(H_2O)$, $Pb_2Ge(SeO_3)_4$ and $BiFe(SeO_3)_3$ indicate that they are transparent in the range of 4000–1000 cm^{-1} (2.5–10 μm) (Fig. S3†). The IR absorption bands of Se–O, Te–O and Ge–O vibrations appeared between 400 and 1000 cm^{-1}. The bands at 420–505 cm^{-1} and 620–870 cm^{-1} can be assigned to the characteristic stretching of Se–O or Te–O bonds. The band at 543 cm^{-1} for $Pb_2Ge(SeO_3)_4$ is the characteristic bending vibration of Ge–O bonds. These assignments are consistent with those previously reported.[25]

UV-visible absorption spectra of the four compounds show little absorption in the range of 800–2500 nm (0.8–2.5 μm) (Fig. S4†). Optical diffuse reflectance spectrum studies indicate that $Pb_3(TeO_3)Cl_4$, $Pb_3(SeO_3)_2Br_2$, $Pb_2Cd_3(SeO_3)_4I_2(H_2O)$, $Pb_2Ge(SeO_3)_4$ and $BiFe(SeO_3)_3$ are semiconductors with optical band gaps of 3.79, 3.73, 3.42, 4.10 and 2.54 eV, respectively (Fig. S5†).

Since $Pb_3(TeO_3)Cl_4$ and $BiFe(SeO_3)_3$ crystallized in noncentrosymmetric space groups, it is worth studying their SHG properties. SHG measurements on a 1064 nm Q-switch laser with the sieved powder samples revealed that no signal was observed for $Pb_3(TeO_3)Cl_4$, whereas $BiFe(SeO_3)_3$ displays a weak SHG signal of about 0.2 × KDP (Fig. 6). The weak or no SHG responses for $BiFe(SeO_3)_3$ and $Pb_3(TeO_3)Cl_4$ may be related to their crystal structures. Firstly, the lone pairs of Pb and Bi atoms in both compounds are inert. Hence the polarizations are mainly from the tellurite and selenite anions. In $Pb_3(TeO_3)Cl_4$, the TeO_3 groups exhibit two types of orientations. The individual dipole moment of one anion is pointed along [00−1] whereas that of the other one points in the [001] direction approximately. Thus, the polarization associated with the two types of $Te(1)O_3$ groups are pointed in opposite directions, with zero net polarizations (Fig. S6a†). In $BiFe(SeO_3)_3$, there are three unique SeO_3 groups. $Se(1)O_3$ and $Se(2)O_3$ groups display two orientations (Fig. S6b†). The polarizations of $Se(1)O_3$ groups orientated towards the [−20−1] and [201] directions while those of the $Se(2)O_3$ groups are in the [−102] and [10−2] directions, resulting in a net polarization of zero. $Se(3)O_3$ groups exhibit four orientations, the polarizations of which are pointed in the [101], [−10−1], [−101] and [10−1] directions, respectively. So, the dipole moments of these SeO_3 are cancelled. In a few words, the individual dipole moments of TeO_3 or SeO_3 groups in the two compounds have been mostly cancelled out, resulting in the observation of no or weak SHG signal.

Thermogravimetric analyses (TGA)

TGA analyses under a nitrogen atmosphere indicate that $Pb_3(TeO_3)Cl_4$, $Pb_3(SeO_3)_2Br_2$, $Pb_2Cd_3(SeO_3)_4I_2(H_2O)$, $Pb_2Ge(SeO_3)_4$ and $BiFe(SeO_3)_3$ are stable up to 530, 530, 380, 345 and 445 °C, respectively (Fig. 7).

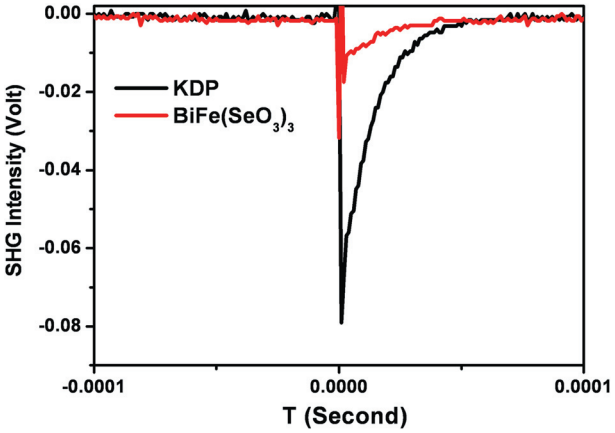

Fig. 6 Oscilloscope traces of SHG signals of $BiFe(SeO_3)_3$ and KDP (reference).

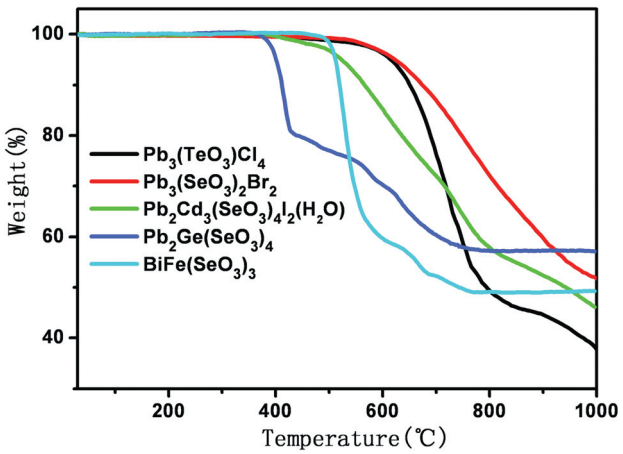

Fig. 7 TGA diagrams for $Pb_3(TeO_3)Cl_4$, $Pb_3(SeO_3)_2Br_2$, $Pb_2Cd_3(SeO_3)_4I_2(H_2O)$, $Pb_2Ge(SeO_3)_4$ and $BiFe(SeO_3)_3$.

$Pb_3(TeO_3)Cl_4$ and $Pb_3(SeO_3)_2Br_2$ each exhibit one main step of weight loss in the temperature ranges of 530–1000 and 530–1000 °C, corresponding to the release of TeO_2 or SeO_2 and halogen gases or elements. From the slopes of the curves, it is obvious that the decompositions of the three compounds were not completed. The observed weight losses are 63.4% and 48.2% at 1000 °C.

$Pb_2Cd_3(SeO_3)_4I_2(H_2O)$ exhibits a very small weight loss at around 50 °C, which can be ascribed to the loss of lattice water (Fig. S10†). Then it displays a main weight loss in the temperature range of 380–1000 °C, corresponding to the release of SeO_2 and halogen gases or elements during the decomposition. The total weight loss observed at 1000 °C is 53.9%.

$Pb_2Ge(SeO_3)_4$ and $BiFe(SeO_3)_3$ are stable up to 345 and 445 °C, respectively, then they exhibit one step of weight loss in the temperature ranges of 345–790 and 445–770 °C, respectively. For $Pb_2Ge(SeO_3)_4$, the observed weight loss of 42.8% can be attributed to the release of 4 mol of SeO_2 per formula unit, which is slightly smaller than the calculated one (44.6%). For

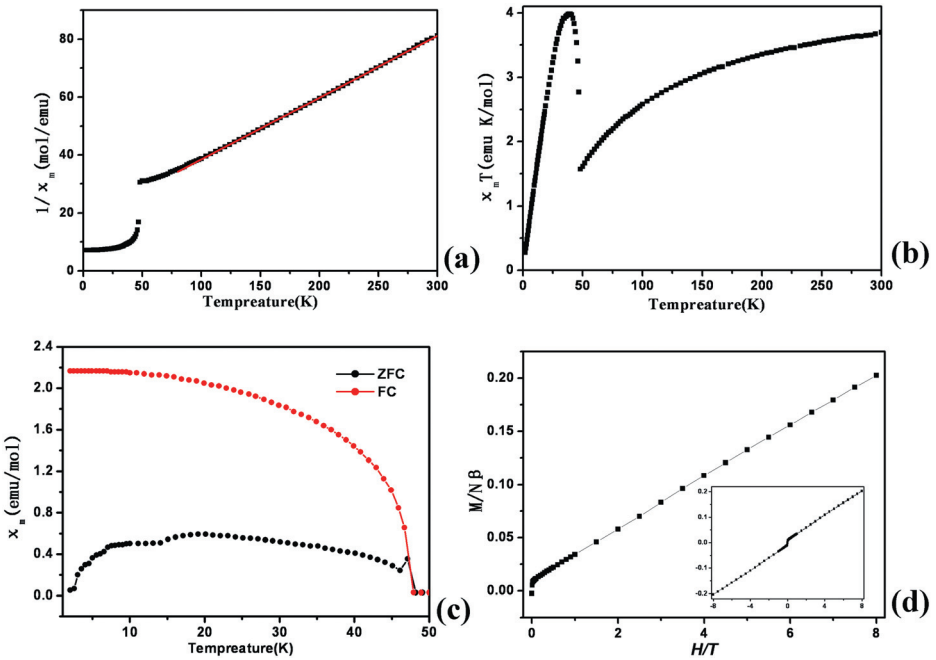

Fig. 8 Plots of $1/\chi_M$ *vs.* T (H = 1000 Oe) (a) and $\chi_M T$ *vs.* T (b); field cooled (FC) and zero-field cooled (ZFC) plot of χ_M *vs.* T at H = 50 Oe (c); M *vs.* H plot at 2 K (d).

$BiFe(SeO_3)_3$, the observed weight loss at 770 °C of 50.9% is close to the calculated one (51.6%). The final residuals were not characterized due to their melting with the TGA bucket made of Al_2O_3 under such high temperatures.

Magnetic measurement

The temperature-dependent magnetic susceptibilities of $BiFe(SeO_3)_3$ were measured on a powder crystalline sample at 1000 Oe in the temperature range of 2–300 K.

The plot of $1/\chi_M$ *vs.* T above 100 K could be fit according to the Curie–Weiss law ($\chi_M = C/(T - \theta)$), which gave a Weiss constant, $\theta = -81.2$ K and a Curie constant, $C = 4.76$ emu mol^{-1}. The very negative Weiss constant suggests strong antiferromagnetic interaction between neighboring Fe^{3+} ions (Fig. 8a). At 300 K, the $\chi_M T$ value is 3.70 emu mol^{-1} K, which corresponds to an effective magnetic moment (μ_{eff}) of 5.44 μ_B for one isolated Fe^{3+} ion. Upon cooling, the $\chi_M T$ value decreases continuously due to antiferromagnetic coupling. A sharp increase occurs near *ca.* 48 K, reaching a maximum of 3.99 emu mol^{-1} K at *ca.* 38 K, suggesting the onset of long range order with a spontaneous magnetization, possibly caused by ferrimagnetism or canted antiferromagnetism.[26] The ordering was verified by zero-field-cooled (ZFC) and field-cooled (FC) measurements, which showed a bifurcation below a temperature of *ca.* 47 K (Fig. 8c). Furthermore, the temperature dependence of the FC magnetization in the range of 50–5000 Oe showed a strong field dependence of the magnetic susceptibility below *ca.* 47 K (Fig. S7†), confirming the existence of long-range magnetic order. Below *ca.* 38 K, the $\chi_M T$ decreases down to 2 K with a value of 1.81 emu mol^{-1} K, owing to increasing antiferromagnetic interactions and/or saturation effects.[26] The field-cooled $\chi_M T$ values at different applied fields as a function of temperature show a spontaneous increase around 48 K, and it is more noticeable for lower field strengths (Fig. S7†). Thus, the second drop in $\chi_M T$ below 38 K may be due to the magnetic field saturation effect.[26]

To clarify the nature of the magnetic behavior at low temperatures, we have measured the isothermal magnetization at 2 K with fields up to 8 T (Fig. 8d). The magnetization shows a sharp increase at low fields and a linear variation at $H > 0.02$ T. At 8 T, the magnetization value reaches 0.20 μ_B per Fe(III) ion, far from the saturation values of $M_S = 5.92$ μ_B for a spin-only Fe(III) ion, indicating the antiferromagnetic coupling between the Fe(III) ions. Combining with the measurement results of ZFC and FC with the isothermal magnetization, it can be concluded that $BiFe(SeO_3)_3$ displays weakly ferromagnetic behavior originating from spin canting.[27]

It is well known that the occurrence of spin canting is usually caused by either single ion magnetic anisotropy or antisymmetric exchange in magnetic entities.[27] Due to the negligible single ion anisotropy for high spin Fe^{3+}, the observation of the spin canting in $BiFe(SeO_3)_3$ should arise from the antisymmetric magnetic exchange, which is related to the antisymmetric nature of the magnetic entities. $BiFe(SeO_3)_3$ crystallizes in a non-centrosymmetric space group, $P2_12_12_1$, which is in the absence of an inversion center between the neighboring Fe^{3+} ions and the spin-canting in the structure may arise from the Dzyaloshinsky–Moriya (D–M) interaction.[28] Such spin-canting effects arising from the antisymmetric exchange interaction have been observed in some isotropic Fe^{3+} and Mn^{2+} complexes.[29]

Theoretical studies

To further understand the chemical bonding and electronic structures of the five compounds, band structures as well as DOS

calculations, based on the DFT method, were done using the computer code CASTEP.[21]

The calculated band structures of the five compounds along with high symmetry points of the first Brillouin zone are plotted in Fig. S8.† The state energies (eV) of the lowest conduction band (LCB) and the highest valence band (HVB) of the compounds are listed in Table S1.† It is revealed that $Pb_3(TeO_3)Cl_4$, $Pb_2Cd_3(SeO_3)_4I_2(H_2O)$ and $BiFe(SeO_3)_3$ exhibit direct band gaps of 3.20, 3.11 and 0.68 eV, whereas $Pb_3(SeO_3)_2Br_2$ and $Pb_2Ge(SeO_3)_4$ are indirect band-gap crystals with band gaps of 3.25 and 3.06 eV. The calculated band gaps of these compounds are smaller than the corresponding experimental ones (3.79, 3.73, 3.42, 4.10 and 2.54 eV, respectively for $Pb_3(TeO_3)Cl_4$, $Pb_3(SeO_3)_2Br_2$, $Pb_2Cd_3(SeO_3)_4I_2(H_2O)$, $Pb_2Ge(SeO_3)_4$ and $BiFe(SeO_3)_3$), which is due to the limitation of the DFT method that usually underestimates the band gap of semiconductors and insulators.[30]

The bands can be assigned according to the total and partial DOS as plotted in Fig. S9.† For $Pb(TeO_3)Cl_4$ (Fig. S9a†), the VBs between −20.0 and − 12.5 eV are mainly from O 2s, Cl 2s and Pb 5d states mixing with Se 4s and Se 4p states. The VBs between −10.0 and −5.0 eV are mainly from Te 5s states as well as O 2p states. We will focus on the Fermi level region (between −5.0 and 7.5 eV), which counts for most of the bonding character in a compound. It is obvious that O 2p states dominate the whole Fermi level region and the Cl 3p states cover the region between −3.0 and 0 eV. In the regions of −5.0 to −3.0 and 2.5 to 7.5 eV, Te 5p states overlap fully with O 2p, indicating the well-defined Te–O covalent interactions. For other compounds, the PDOSs of the anion groups behave generally similar to $Pb(TeO_3)Cl_4$. The only differences are the states' positions of cations (Fe, Cd and Ge).

In addition, the bond orders of all chemical bonds in the five compounds have been calculated. The bond orders of Pb–O, Pb–Cl, Pb–Br, Pb–I, Cd–O, Ge–O, Fe–O, Te–O and Se–O are 0.04–0.18 e, 0.03–0.18 e, 0.15 e, 0.06 e, 0.11–0.22 e, 0.34–0.40 e, 0.27–0.31 e, 0.39–0.43 e and 0.27–0.56 e (that of standard a covalent single bond is generally 1.0 e), respectively. The bond orders reveal that the covalent character of the bonds in these compounds have the following order: Se–O (Te–O and Ge–O) > Cd–O (Fe–O) > cation–O/Cl (Pb–O, Bi–O, and Pb–X). These results are in accordance with those deduced from DOSs.

Conclusions

In summary, four new lead(II) and bismuth(III) selenites and a tellurite, namely, $Pb_3(TeO_3)Cl_4$, $Pb_3(SeO_3)_2Br_2$, $Pb_2Cd_3(SeO_3)_4I_2(H_2O)$, $Pb_2Ge(SeO_3)_4$ and $BiFe(SeO_3)_3$, have been prepared and structurally characterized. We have introduced halide anions (Cl^-, Br^- and I^-) or cations (Cd^{2+}, Ge^{4+} and Fe^{3+}) into the lead(II) or bismuth(III) selenites and tellurites successfully. The roles of halide ions and the additional metal ions are quite distinct from each other. It is observed that the QO_3/X molar ratio has a dramatic effect on the structure of the compound formed. When the QO_3/X molar ratio is smaller than 1.0, the structure will be dominated by lead(II) halide subunits, whereas a larger QO_3/X molar ratio than 1.0 will lead to a metal selenite-dominated structure. The introduction of Ge^{4+}, Fe^{3+} and Cd^{2+} into the lead(II) or bismuth(III) selenites and tellurites can also give a variety of new compounds with rich structural types. Among these compounds, $Pb_3(TeO_3)Cl_4$ and $BiFe(SeO_3)_3$ are noncentrosymmetric, crystallizing in space groups $Pna2_1$ and $P2_12_12_1$, respectively, but unfortunately their SHG responses are very weak. $BiFe(SeO_3)_3$ displays interesting magnetic properties. Our future research efforts will be devoted to the explorations of new SHG compounds by the introduction of other lone pair cations, such as Sn^{2+} and Sb^{3+}, into the metal selenite and tellurite systems.

Acknowledgements

This work was supported by National Natural Science Foundation of China (Nos. 20731006, 20825104, and 20101107) and the Knowledge Innovation Program of the Chinese Academy of Sciences.

Notes and references

1 M. S. Wickleder, *Chem. Rev.*, 2002, **102**, 2011 and references therein.
2 (*a*) S.-H. Kim, J. Yeon and P. S. Halasyamani, *Chem. Mater.*, 2009, **21**, 5335; (*b*) K.-M. Ok, N. S. P. Bhuvanesh and P. S. Halasyamani, *Inorg. Chem.*, 2001, **40**, 1978; (*c*) F. Kong, S. P. Huang, Z. M. Sun, J. G. Mao and W. D. Cheng, *J. Am. Chem. Soc.*, 2006, **128**, 7750; (*d*) Y. Porter, K. M. Ok, N. S. P. Bhuvanesh and P. S. Halasyamani, *Chem. Mater.*, 2001, **13**, 1910; (*e*) M. K. Kim, S.-H. Kim, H.-Y. Chang, P. S. Halasyamani and K. M. Ok, *Inorg. Chem.*, 2010, **49**, 7028.
3 (*a*) J. G. Mao, H. L. Jiang and F. Kong, *Inorg. Chem.*, 2008, **47**, 8498; (*b*) K. M. Ok and P. S. Halasyamani, *Chem. Mater.*, 2006, **18**, 3176; (*c*) P. S. Halasyamani, *Chem. Mater.*, 2004, **16**, 3586; (*d*) H.-S. Ra, K.-M. Ok and P. S. Halasyamani, *J. Am. Chem. Soc.*, 2003, **125**, 7764; (*e*) H. Y. Chang, S.-H. Kim, K.-M. Ok and P. S. Halasyamani, *Chem. Mater.*, 2009, **21**, 1654; (*f*) H. Y. Chang, S. W. Kim and P. S. Halasyamani, *Chem. Mater.*, 2010, **22**, 3241.
4 (*a*) V. Balraj and K. Vidyasagar, *Inorg. Chem.*, 1999, **38**, 5809; (*b*) V. Balraj and K. Vidyasagar, *Inorg. Chem.*, 1998, **37**, 4764; (*c*) W. T. A. Harrison, L. L. Dussack and A. J. Jacobson, *Inorg. Chem.*, 1994, **33**, 6043; (*d*) Y. Porter and P. S. Halasyamani, *J. Solid State Chem.*, 2003, **174**, 441; (*e*) Y.-U. Kwon, K.-S. Lee and Y. H. Kim, *Inorg. Chem.*, 1996, **35**, 1161; (*f*) K. M. Ok and P. S. Halasyamani, *Inorg. Chem.*, 2005, **44**, 3919; (*g*) Q.-H. Gu, C.-L. Hu, J.-H. Zhang and J.-G. Mao, *Dalton Trans.*, 2011, **40**, 2562.
5 (*a*) T. Sivakumar, K. M. Ok and P. S. Halasyamani, *Inorg. Chem.*, 2006, **45**, 3602; (*b*) W. T. A. Harrison, L. L. Dussack and A. J. Jacobson, *J. Solid State Chem.*, 1996, **125**, 234; (*c*) J. Y. Hou, C. C. Huang, H. H. Zhang, Q. Y. Yang, Y.-P. Chen and J.-F. Xu, *Acta Crystallogr. C*, 2005, **61**, i59; (*d*) J. Y. Hou, C. C. Huang, H. H. Zhang, C. Y. Tu, R. Q. Sun and Q. Y. Yang, *J. Mol. Struct.*, 2006, **785**, 37; (*e*) S.-Y. Zhang, C.-L. Hu, C.-F. Sun and J.-G. Mao, *Inorg. Chem.*, 2010, **49**, 11627.
6 (*a*) S. Y. Zhang, H. L. Jiang, C. F. Sun and J. G. Mao, *Inorg. Chem.*, 2009, **48**, 11809; (*b*) H. L. Jiang, Z. Xie and J. G. Mao, *Inorg. Chem.*, 2007, **46**, 6495; (*c*) Y. Laligant, *J. Solid State Chem.*, 2001, **160**, 401; (*d*) D. Zhang and M. Johnsson, *Acta Crystallogr. C*, 2009, **65**, i9.
7 (*a*) Y. Zhou, C. L. Hu, T. Hu, F. Kong and J. G. Mao, *Dalton Trans.*, 2009, 5747; (*b*) H. L. Jiang, S. P. Huang, Y. Fan and J. G. Mao, *Chem.–Eur. J.*, 2008, **14**, 1972; (*c*) H. L. Jiang, F. Kong, Y. Fan and J. G. Mao, *Inorg. Chem.*, 2008, **47**, 7430; (*d*) D. Pitzschke and M. Jansen, *Z. Anorg. Allg. Chem.*, 2007, **633**, 1563; (*e*) J. Ling and T. E. Albrecht-Schmitt, *J. Solid State Chem.*, 2007, **180**, 1601; (*f*) S. D. Nguyen, S.-H. Kim and P. S. Halasyamani, *Inorg. Chem.*, 2011, **50**, 5215.
8 (*a*) F. Kong, C. L. Hu, T. Hu, Y. Zhou and J. G. Mao, *Dalton Trans.*, 2009, 4962; (*b*) K. M. Ok and P. S. Halasyamani, *Chem. Mater.*, 2002, **14**, 2360; (*c*) D. W. Lee, S.-J. Oh, P. S. Halasyamani and K. M. Ok, *Inorg. Chem.*, 2011, **50**, 4473.
9 (*a*) Y. L. Shen, H. L. Jiang, J. Xu, J. G. Mao and K. W. Cheah, *Inorg. Chem.*, 2005, **44**, 9314; (*b*) H. L. Jiang, E. Ma and J. G. Mao, *Inorg. Chem.*, 2007, **46**, 7012; (*c*) P.-X. Li, S.-Y. Zhang and J.-G. Mao, *Dalton*

Trans., 2010, **39**, 11560; (*d*) S.-Y. Zhang and J.-G. Mao, *Inorg. Chem.*, 2011, **50**, 4934.
10 (*a*) S.-H. Kim, J. Yeon and P. S. Halasyamani, *Chem. Mater.*, 2009, **21**, 5335; (*b*) S. V. Krivovichev, E. Y. Avdontsev and P. C. Burns, *Z. Anorg. Allg. Chem.*, 2004, **630**, 558; (*c*) K. M. Ok, N. S. P. Bhuvanesh and P. S. Halasyamani, *Inorg. Chem.*, 2001, **40**, 1978; (*d*) O. A. Dityatyev, P. Smidt, S. Y. Stefanovich, P. Lightfoot, V. A. Dolgikh and H. Opperman, *Solid State Sci.*, 2004, **6**, 915; (*e*) Y. Porter, S. P. N. Bhuvanesh and P. S. Halasyamani, *Inorg. Chem.*, 2001, **40**, 1172.
11 (*a*) J. Yeon, S.-H. Kim, M. A. Hayward and P. S. Halasyamani, *Inorg. Chem.*, 2011, **50**, 8663; (*b*) H. Effenberger, *J. Solid State Chem.*, 1988, **73**, 118; (*c*) M. G. Johnston and W. T. A. Harrison, *J. Solid State Chem.*, 2004, **177**, 4680; (*d*) H. Effenberger, *Acta Chem. Scand.*, 1996, **50**, 967; (*e*) H. Effenberger, *J. Alloys Compd.*, 1998, **281**, 152; (*f*) K. M. Ok and P. S. Halasyamani, *Solid State Sci.*, 2002, **4**, 793.
12 (*a*) P. Millet, B. Bastide, V. Pashchenko, S. Gnatchenko, V. Gapon, Y. Ksari and A. Stepanov, *J. Mater. Chem.*, 2001, **11**, 1152; (*b*) R. Becker and M. Johnsson, *Solid State Sci.*, 2005, **7**, 375; (*c*) S. V. Krivovichev and S. K. Filatov, *Can. Mineral.*, 2006, **44**, 507.
13 (*a*) M. Johnsson, K. W. Törnroos, F. Mila and P. Millet, *Chem. Mater.*, 2000, **12**, 2853; (*b*) M. Johnsson, K. W. Törnroos, P. Lemmens and P. Millet, *Chem. Mater.*, 2003, **15**, 68; (*c*) P. Millet, M. Johnsson, V. Pashchenko, Y. Ksari, A. Stepanov and F. Mila, *Solid State Ionics*, 2001, **141**, 559.
14 (*a*) D. Zhang, H. Berger, R. K. Kremer, D. Wulferding, P. Lemmens and M. Johnsson, *Inorg. Chem.*, 2010, **49**, 9683; (*b*) H.-L. Jiang and J.-G. Mao, *Inorg. Chem.*, 2006, **45**, 7593; (*c*) R. Becker, M. Johnsson, R. K. Kremer, H.-H. Klauss and P. Lemmens, *J. Am. Chem. Soc.*, 2006, **128**, 15469; (*d*) D. Zhang, M. Johnsson, H. Berger, R. K. Kremer, D. Wulferding and P. Lemmens, *Inorg. Chem.*, 2009, **48**, 6599.
15 (*a*) Y. Porter and P. S. Halasyamani, *Inorg. Chem.*, 2003, **42**, 205; (*b*) D. O. Charkin, O. S. Morozov, E. A. Ul'yanova, P. S. Berdonosov, V. A. Dolgikh, C. Dickinson, W. Z. Zhou and P. Lightfoot, *Solid State Sci.*, 2006, **8**, 1029; (*c*) Y. Porter and P. S. Halasyamani, *Inorg. Chem.*, 2001, **40**, 2640; (*d*) F. Demartin, C. M. Gramaccioli and T. Pilati, *Can. Mineral.*, 2003, **41**, 1147.
16 (*a*) P. S. Berdonosov, S. Yu. Stefanovitch and V. A. Dolgikh, *J. Solid State Chem.*, 2000, **149**, 236; (*b*) S. A. Ibragimov, P. S. Berdonosov, V. A. Dolgikh, D. Q. Huong and H. Oppermann, *Inorg. Mater.*, 2002, **38**, 1291; (*c*) P. S. Berdonosov, D. O. Charkin, A. M. Kusainova, C. H. Hervoches, V. A. Dolgikh and P. Lightfoot, *Solid State Sci.*, 2000, **2**, 553; (*d*) L. N. Kholodkovsaya, V. A. Dolgikh and B. A. Popovkin, *J. Solid State Chem.*, 1995, **116**, 406; (*e*) V. A. Dolgikh, L. N. Kholodkovskaya and B. A. Popovkin, *Russ. J. Inorg. Chem.*, 1996, **41**, 932; (*f*) M. K. Kim, V. Jo, D. W. Lee and K. M. Ok, *Dalton Trans.*, 2010, **39**, 6037; (*g*) M. Ruck and P. Schmidt, *Z. Anorg. Allg. Chem.*, 2003, **629**, 2133.
17 W. M. Wendlandt and H. G. Hecht, *Reflectance Spectroscopy*, Interscience, New York, 1966.
18 S. K. Kutz and T. T. Perry, *J. Appl. Phys.*, 1968, **39**, 3798.
19 E. A. Boudreaux and L. N. Mulay, ed., *Theory and Applications of Molecular Paramagnetism*, John Wiley & Sons, New York, 1976.
20 (*a*) *CrystalClear, Version 1.3.5*, Rigaku Corp., Woodlands, TX, 1999; (*b*) G. M. Sheldrick, *SHELXTL, Crystallographic Software Package, SHELXTL, Version 5.1*, Bruker-AXS, Madison, WI, 1998; (*c*) A. L. Spek, *J. Appl. Crystallogr.*, 2003, **36**, 7.
21 (*a*) M. D. Segall, P. J. D. Lindan, M. J. Probert, C. J. Pickard, P. J. Hasnip, S. J. Clark and M. C. Payne, *J. Phys.: Condens. Matter*, 2002, **14**, 2717; (*b*) V. Milman, B. Winkler, J. A. White, C. J. Pickard, M. C. Payne, E. V. Akhmatskaya and R. H. Nobes, *Int. J. Quantum Chem.*, 2000, **77**, 895.
22 J. S. Lin, A. Qteish, M. C. Payne and V. Heine, *Phys. Rev. B*, 1993, **47**, 4174.
23 J. P. Perdew, K. Burke and M. Ernzerhof, *Phys. Rev. Lett.*, 1996, **77**, 3865.
24 (*a*) A. Guesdon and B. Raveau, *Chem. Mater.*, 2000, **12**, 2239; (*b*) E. O. Chi, K. M. Ok, Y. Porter and P. S. Halasyamani, *Chem. Mater.*, 2006, **18**, 2070.
25 (*a*) K. Nakamoto, *Infrared Spectra of Inorganic and Coordination Compounds*, Wiley, New York, 1970; (*b*) V. P. Verma, *Thermochim. Acta*, 1999, **327**, 63.
26 (*a*) M. Yang, J. Yu, L. Shi, P. Chen, G. H. Li, Y. Chen, R. R. Xu and S. Gao, *Chem. Mater.*, 2006, **18**, 476; (*b*) A. Chippindale, F. M. Gaslain, A. D. Bond and A. V. Powell, *J. Mater. Chem.*, 2003, **13**, 1950.
27 (*a*) R. L. Carlin, *Magnetochemistry*, Springer-Verlag, Berlin, 1986; (*b*) F. Sanz, C. Parada, J. M. Rojo and C. Ruiz-Valero, *Chem. Mater.*, 2001, **13**, 1334; (*c*) M. Riou-Cavellec, C. Lesaint, M. Nogues, J. M. Greneche and G. Ferey, *Inorg. Chem.*, 2003, **42**, 5669; (*d*) S. Merchant, J. N. McElearney, G. E. Shankle and R. L. Carlin, *Physica*, 1974, **78**, 308.
28 (*a*) R. L. Carlin and A. J. Van-Duyneveldt, *Magnetic Properties of Transition Metal Compounds*, Springer-Verlag, New York, 1977; (*b*) H.-B. Xu, Z.-M. Wang, L. Tao and S. Gao, *Inorg. Chem.*, 2007, **46**, 3089.
29 (*a*) E. Q. Gao, Y. F. Yue, S. Q. Bai, Z. He, S. W. Zhang and C. H. Yan, *Chem. Mater.*, 2004, **16**, 1590; (*b*) Z. M. Wang, B. Zhang, T. Otsuka, K. Inoue, H. Kobayashi and M. Kurmoo, *Dalton Trans.*, 2004, 2209; (*c*) D. Armentano, G. De Munno, T. F. Mastropietro, M. Julve and F. Lloret, *J. Am. Chem. Soc.*, 2005, **127**, 10778, and references therein; (*d*) W. Li, H. P. Jia, Z. F. Ju and J. Zhang, *Dalton Trans.*, 2008, 5350.
30 (*a*) R. W. Godby, M. Schluther and L. Sham, *Phys. Rev. B*, 1987, **36**, 6497; (*b*) C. M. I. Okoye, *J. Phys.: Condens. Matter*, 2003, **15**, 5945; (*c*) R. Terki, G. Bertrand and H. Aourag, *Microelectron. Eng.*, 2005, **81**, 514; (*d*) H.-L. Jiang, F. Kong and J.-G. Mao, *J. Solid State Chem.*, 2007, **180**, 1764.

